The International Journal of Advanced Manufacturing Technology (2025) 136:729–744
https://doi.org/10.1007/s00170-024-14853-5

ORIGINAL ARTICLE

# Influence of the manufacturing strategy on the microstructure and mechanical properties of Invar 36 alloy parts manufactured by CMT-WAAM

**Amaia Iturrioz[1,2] · Eneko Ukar[2] · Juan Carlos Pereira[1]**

Received: 5 July 2024 / Accepted: 20 November 2024 / Published online: 6 December 2024


## Abstract

The influence of the manufacturing strategy of Invar 36 alloy parts manufactured by Directed Energy Deposition by Arc (DED-Arc) also known as wire and arc additive manufacturing (WAAM) using cold metal transfer (CMT) technology has been investigated. This study focuses on the influence of applying different deposition strategies on the resulting microstructure and mechanical properties. As manufacturing costs and time are critical issues which determine the business case in WAAM applications, it is important to use the smallest possible amount of feedstock material. Therefore, different manufacturing strategies are used to obtain the variable wall thicknesses required for each part preform using WAAM as a manufacturing route. Differences in manufacturing temperature and thermal history due to different deposition strategies have been recorded. Deep microstructural analysis in as-built condition revealed that granular alignment and the crystallographic texture obtained differ between deposition strategies studied. This is the reason why there are differences in the mechanical properties, such as yield strength, ultimate tensile strength, elongation, and hardness, of the different strategies analyzed. The results revealed that the higher strength is obtained in three overlapped weld beads for the walls (514 and 581 MPa in building direction and perpendicular direction, respectively), compared to single weld bead wall (481 and 489 MPa), circular single weld bead wall (460 and 484 MPa), and meandering weld bead wall (467 and 439 MPa). The opposite is true for elongation, which is a typical correlation between strength and ductility in Fe-based alloys, having the highest elongation in the meandering weld bead wall (26 and 30%) and circular single weld bead (30 and 27%) compared to single weld bead wall (27 and 23%) and three overlapped weld bead wall (23 and 20%). It can therefore be concluded that an Invar 36 alloy part manufactured by CMT-WAAM with different strategies will have different mechanical properties, having a difference in ultimate tensile strength of 54 MPa and 142 MPa, and in elongation of 7% and 10% in building direction and perpendicular direction, respectively, between the most and the least resistant zone.

**Keywords** WAAM · Invar 36 · Manufacturing strategies · Mechanical properties · Microstructure

## Glossary

| | |
|---|---|
| AM | Additive manufacturing |
| DED-Arc | Directed Energy Deposition by Arc |
| WAAM | Wire and arc additive manufacturing |
| CMT | Cold metal transfer |
| LMD | Laser metal deposition |
| EBAM | Electron beam additive manufacturing |
| BTF | By-to-fly |
| PAW | Plasma arc welding |
| GMAW | Gas metal arc welding |
| YS | Yield strength (MPa) |
| UTS (Rm) | Ultimate tensile strength (MPa) |
| e | Elongation (%) |
| HI | Heat input (KJ/cm) |
| I | Current (A) |
| V | Voltage (V) |
| TS | Travel speed (mm/s) |
| CTE | Coefficient of thermal expansion |
| FEG-SEM | Field emission gun scanning electron microscopy |
| EBSD | Electron backscatter diffraction |

✉ Amaia Iturrioz
aiturrioz@lortek.es; aiturrioz011@ikasle.ehu.eus

[1] LORTEK Technological Centre, Basque Research and Technology Alliance (BRTA), Arranomendia Kalea 4A, 20240 Ordizia, Gipuzkoa, Spain

[2] Department of Mechanical Engineering, University of the Basque Country (UPV/EHU), Ingeniero , Torres Quevedo Plaza, 1, 48013 Bilbao, Bizkaia, Spain

EDS Energy dispersive spectroscopy
LOM Light optical microscopy

## 1 Introduction

According to ISO/ASTM 52900 standard [1], Directed Energy Deposition (DED) is the additive manufacturing (AM) process that uses a focused thermal energy source (laser, electron beam, or plasma arc) to fuse materials as they are deposited. DED technology covers multiple direct metal deposition processes according to the thermal source used, such as laser metal deposition (LMD), wire and arc additive manufacturing (WAAM), and electron beam additive manufacturing (EBAM) [2]. Among these processes, DED-Arc or better known as WAAM process that utilizes an electric arc to melt the wire feedstock has been chosen for this work. WAAM is a key process for improved design and manufacturing of near-net-shape parts. In fact, some recent progresses are published recently by some authors [3–5]. WAAM is an additive manufacturing technology oriented to large and low to medium complexity components, where the deposition of overlapped layers is used to obtain near-net-shape parts. The main advantages and disadvantages of this technology are compiled in Table 1.

In this work, the cold metal transfer (CMT) welding technique from Fronius Company [7] has been used. CMT is an evolution of the conventional dip transfer arc welding process. In the conventional process when the short circuit occurs, the increasing current breaks the short circuit allowing the arc ignition. However, in the CMT process when the short circuit occurs, the alternating wire forward and retraction movement produces a more controlled droplet detachment and reignition. This reversing wire motion takes place at a high frequency (50 to 170 Hz) [7]. The advantages of this evolution are that the metal transference is spatter-free, the high stability of the electric arc, and hence a more controlled microstructure [7]. Apart from these advantages, CMT also reduces the heat input, reducing the residual stresses and distortion and avoiding a collapse of the building [8]. Apart from that, increasing heat input decreases mechanical properties, caused by the higher heat accumulation and lower cooling rate that increases grain size [9].

The advantage of the obtention of near-net-shape parts is the material saving, which is interesting for the molding sector among others, and more generally in terms of sustainability. Typically used material used in molds for the fabrication of aeronautics and astronautics composite structures is Invar 36 (FeNi36) due to its low or nearly zero thermal coefficient [10] (1.2 ppm/°C, ordinary steels have values of around 11–15 ppm/°C) [11], which is beneficial to accomplish tight tolerances of molded components. Nowadays, machining is the most common manufacturing process for Invar 36 alloy, but this process presents some problems due to its high ductility (0.06–0.45), low conductivity (12–15 W/m K), and the work hardening, which results in high tool wear during machining [12]. Near-net-shape manufacturing allowed by WAAM reduces in a significant way the material to machine, enabling low by-to-fly ratios (BTF ratio).

Invar 36 alloy is also used in applications that need high dimensional stability, such as precision instruments, valves in motors, and structural components in the electronics field. Additionally, this alloy presents high corrosion strength, making it interesting for liquefied natural gas containers and pipelines for long-distance transportation [10].

The typical microstructure of Invar 36 is single austenite (at room temperature), and its mechanical properties are high elongation with a low hardness value and a lower Young's modulus than common steels [10]. The WAAM process involves heating and cooling cycles when creating the successive layers and the remelting of the previous layer in the additive process, creating temperature gradients. This affects the resulting microstructure in as-built condition. F. Veiga et al. [12] concluded that either using plasma arc welding (PAW) or gas metal arc welding (GMAW) technologies for the WAAM manufacturing process with Invar 36, grains with a dendritic substructure, are obtained. These grains are columnar grains that grow in the wall-growing direction of deposition. Because the heat dissipation is greater in the edges of the walls, in this zone, equiaxed grains can be observed. In this work, also, mechanical properties are studied, where higher yield strength (YS) and ultimate

**Table 1** Advantages and disadvantages of WAAM technology [6]

| Advantages | Disadvantages |
|---|---|
| Minimum human intervention and setup times when adequate setup and process parameters are selected | High level of Residual stresses and geometry distortion associated with them |
| Commercially available welding equipment and filler metals (used already in welding) | Relatively poor part accuracy and poor surface finish in as-built condition |
| Flexible build robotic cells. No limitation in part size | Need of finishing as milling and grinding |
| High deposition rates compared to other DED processes | Reduced alloys and hi-tech commercial materials available in wire format |
| Low investment cost. Conventional arc welding equipment is used | |

tensile strength (UTS) results are observed in the horizontal specimens due to the anisotropy of the WAAM technology. The hardness results show that the presence of precipitates caused because of the thermal cycles typical of this technology increase hardness locally. In general, the hardness values are comparable to those observed in the material obtained by the conventional method. Arjun et al. [13] studied the influence of the heat input (HI) in the manufacturing of directed energy deposition of Invar 36 alloy blocks using gas tungsten arc welding (GTAW). The results revealed that the microstructure of columnar grains was independent of the HI, but cracking was detected in the highest HI cases. Lowering the HI from 550 to 200 J/mm, the mechanical properties were increased. The analysis of the linear coefficient of thermal expansion (CTE) showed that the effect of different HI was negligible.

Some approaches have been done by the Thesis of Yan Lihao [10]. Two different materials (Invar 36 and mild steel) were used in a mold, where the zone that will be in contact with the part is done by Invar36 taking advantage of its low thermal expansion coefficient property and the base part of the mold was done of mild steel, supplying strength, and saving costs. This bimaterial mold was done by WAAM. The analysis of the joint between the two materials shows that there was no crack or porosity in that area. The tensile test made to the bimaterial samples failed to form the Invar 36 part, remote from the joint, revealing that the Invar was successfully deposited in the steel.

In WAAM, manufacturing strategies have been studied for different feedstock materials and applications [14–18] with the main aim of minimizing the waste of material. Moreover, some components can use different strategies depending on the shape and thickness required in specific zones of the part [18].

These manufacturing strategies can influence the microstructure and hence the obtained mechanical properties [19, 20]. Regarding research works related to manufacturing strategies in WAAM, M. Arana et al. [21] study the influence of the torch movement-based deposition strategies hatching and circling in the final properties of AA2319 aluminium components. They additionally analyzed the influence of deposition geometry by comparing a straight wall and a rectangular wall. It was concluded that the resulting microstructure greatly depends on the deposition strategy and geometry. Y. Suat et al. [9] studied the effect of the parameters and building strategies and correlated with geometrical, metallurgical, and mechanical properties of produced WAAM walls made of low alloyed high-strength steel (ER120S-G). M. Rauch et al. [22] study the influence of the oscillation and parallel strategy on the manufacturing of AA2319 WAAM block structures. It was concluded that a coarse microstructure was observed by the oscillatory strategy having an effect in the tensile properties. B. Cong et al. [23] studied the effect in the porosity, microstructure, and microhardness in thin walls and blocks manufactured by WAAM with AA2319 aluminium alloy. They observe differences in the resulting properties depending on the structures and the CMT process used. L. Vazquez et al. [8] investigate the manufacturing by WAAM-CMT of Ti-6Al-4 V alloy walls with two different building strategies, a single weld bed, and three overlapped weld beads, focusing on the influence of the application of different thermal treatments. They concluded that the anisotropy in elongation was generally lower in the case of the single-bead strategy.

To the best known of authors, there are no publications about specific strategies for the deposition of Invar 36 alloy using WAAM as a manufacturing process. Hang Li et al. [24] studied the microstructure and mechanical properties of Invar 36 alloy fabricated by laser metal deposition (LMD) technology using two different deposition patterns, one-way laser scanning and back-and-forth laser scanning pattern. They concluded that the second scanning pattern results in a higher microhardness and tensile strength, but lower elongation compared to the other deposition pattern.

In this work, the influence of the strategies of the manufacturing by WAAM with Invar 36 has been studied in detail, concretely the microstructure and mechanical and thermal properties, such as yield strength, ultimate tensile strength, elongation, hardness, and coefficient of thermal expansion, which are compared with the values of the material processed by conventional manufacturing methods.

## 2 Materials, equipment, and methods

Invar 36 alloy parts (simple walls of 230 × 130 mm with different thicknesses) were manufactured using a Fronius TPS 400i CMT power source and a Robacta drive CMT WF60i torch from Fronius International, Wels, Austria. The torch was attached to a six-axis ABB robot arm IRB 4600–45/2.05 model indexed to a 2-axis positioner table from ABB, Zürich, Switzerland.

A mixture of Ar and CO2 (2%) was employed as inert shielding gas in the torch. The gas flow was set at 17 L/min [25]. The setup and equipment can be observed in Fig. 1. Welding parameters are included in Table 3. The arc length for the four strategies has been 10 mm. In all cases, the dwell time between the deposition of consecutive layers was 90 s, as reported in other studies in the case of comparing strategies [21]. Table 2 shows the common parameters for the four strategies.

The heat input is calculated following the Eq. 1:

$$HI = \frac{I \times V}{TS} \tag{1}$$

where $I$ is the instantaneous current (A), $V$ is the instantaneous voltage (V), and TS is the travel speed (mm/s). These parameters were previously optimized through experimental

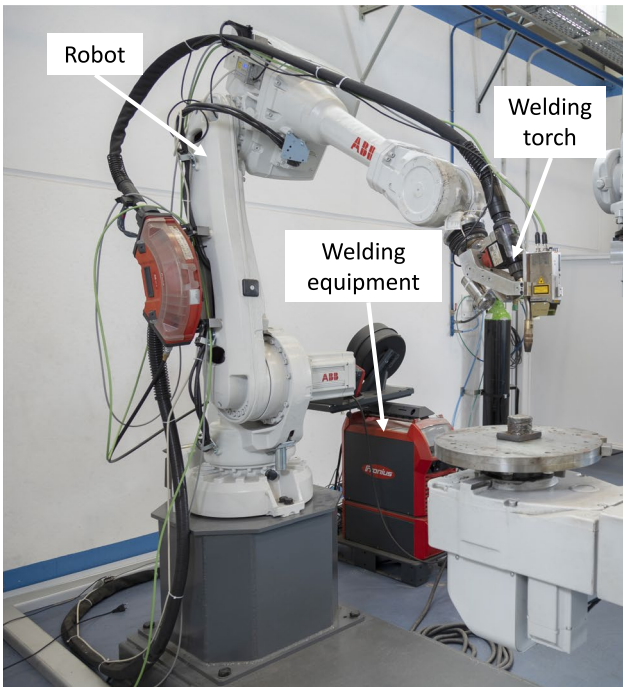


**Fig. 1** Setup for WAAM process, manufacturing equipment, and configuration

**Table 2** Process parameters common to the four strategies

| Shielding gas | Gas flow (L/min) | Arc length (mm) | Dwell time between layers (s) |
|---|---|---|---|
| Ar and CO2 (2%) | 17 | 10 | 90 |

trials for each strategy considering the wall growth stability, the surface finish, dimensional stability, and high deposition rates, using the same methodology used by Rodriguez et al. (Table 3) [6].

As filler metal, a commercial wire of Invar 36 alloy manufactured by VDM with a diameter of 1.2 mm was used. The chemical composition obtained from the ICP analysis is shown in Table 4. Substrates of S235 steel, obtained by hot rolling, with a 10-mm thickness were used for the manufacturing of the different walls. These substrates were clamped to the positioner table.

Four different strategies were evaluated for the manufacturing of the walls. The first strategy (Fig. 2a) consisted in the deposition of a single weld bead per layer. In the second strategy (Fig. 2b), the material deposition was made using a single weld bead per layer but with a circular movement in their trajectory, in which the torch oscillates to generate an overlap of round circles with 1–3 mm amplitude and 2–3 Hz frequency. In the third strategy (Fig. 2c), the deposition of the material was made in a meandering way, with a 3-mm step. And the last strategy (Fig. 2d) consisted in the deposition of three overlapped straight weld beads per layer. The order of the deposition started with the deposition of the middle weld bead, followed by the beads on both sides. For the side beads, the torch tilted 20° from the vertical and the overlapping used was 50% of the width of the weld bead. In all cases, the dwell time between layers was 90 s. The direction of deposition of the weld beads was alternated between layers to avoid the accumulation of material at the arc ignition and extinction zones, that is, the start and end of the single weld bead. All of it allowed a controlled growth of the additive layers that is essential in the WAAM process.

To record the manufacturing temperature between strategies, four K-type thermocouples were attached to the

**Table 3** CMT (cold metal transfer) welding parameters for WAAM parts manufacturing

| Reference | Current (A) | Wire feed speed (m/min) | Voltage (V) | Travel speed (cm/min) | Heat input (KJ/cm) | Time to manufacture a layer (s) | Amplitude (mm) | Frequency (Hz) |
|---|---|---|---|---|---|---|---|---|
| Hatching | 126 | 4.4 | 12.1 | 48 | 1.52 | 28.75 | - | - |
| Circling | 157 | 5.8 | 13 | 48 | 2.04 | 28.75 | 3 | 2 |
| Overlap | 157 | 5.8 | 13 | 48 | 2.04 | 86.26 | 2 | 2 |
| Meandering | 126 | 4.4 | 12.1 | 48 | 1.52 | 210 | 1 | 3 |

**Table 4** Chemical composition of Invar 36 wire feedstock (ICP analysis) and S235 steel build plate (from the provider)

| Materials | Si | Mn | P | Cr | Ni | Mo | Cu | Ti | V | Co | Nb | C | Fe |
|---|---|---|---|---|---|---|---|---|---|---|---|---|---|
| Invar 36 wire | 0.044 | 0.45 | < 0.01 | < 0.1 | 36.2 | < 0.09 | < 0.08 | 0.53 | < 0.05 | < 0.1 | 1.39 | | Balance |
| S235 Steel | < 0.05 | < 0.60 | < 0.04 | < 0.3 | < 0.3 | | < 0.3 | | | | | < 0.22 | Balance |

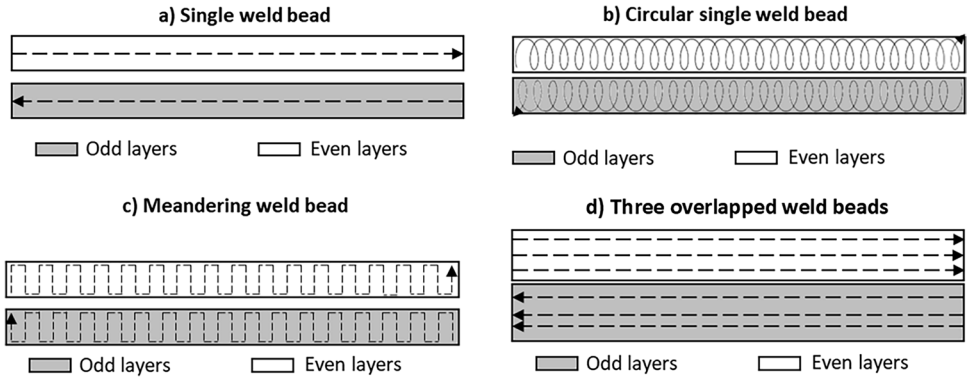


**Fig. 2** Details for the build strategies followed for WAAM walls: **a** single weld bead, (**b**) circular single weld bead, (**c**) meandering weld bead, and (**d**) three overlapped weld beads

substrate using welding, positioned very close to the manufactured wall in the build plate (Fig. 3).

Once the walls were manufactured, ten flat dog-bone tensile test specimens were extracted using the electric discharge machining (EDM) method, five from the horizontal orientation and five from the vertical orientation, as represented in Fig. 4, according to the ASTM E8M standard.

Tensile tests were made in a Z100 ZWICK/Roell model testing machine, ZWICK/Roell, Ulm, Germany, with a maximum load capacity of 100 kN. Specimens were tested at room temperature with a 1.6 mm/min displacement rate and using an extensometer with a 30-mm gauge length.

To perform the characterization of the walls, parts were cut, mounted, grinded, polished, and etched with Nital 5%. Once the samples were prepared, advanced microstructural characterization was done by light microscopy using an Olympus GX51, Olympus, Hamburg, Germany, and by field emission gun scanning electron microscopy (FEG-SEM) using a ZEISS Ultra Plus Field Emission, ZEISS, Overkochen, Germany. IPF (inverse pole figure) maps were generated to analyze the crystallographic texture and grain orientation of the samples. For the generation of the maps, a minimum angle of 5° misorientation was set.

Hardness tests were carried out to find differences between the strategies analyzed. To do so, an EmcoTest Durascan 20 micro-durometer, Emco-Test Prüfmaschinen GmbH, Kuchl, Austria, was used. The number of

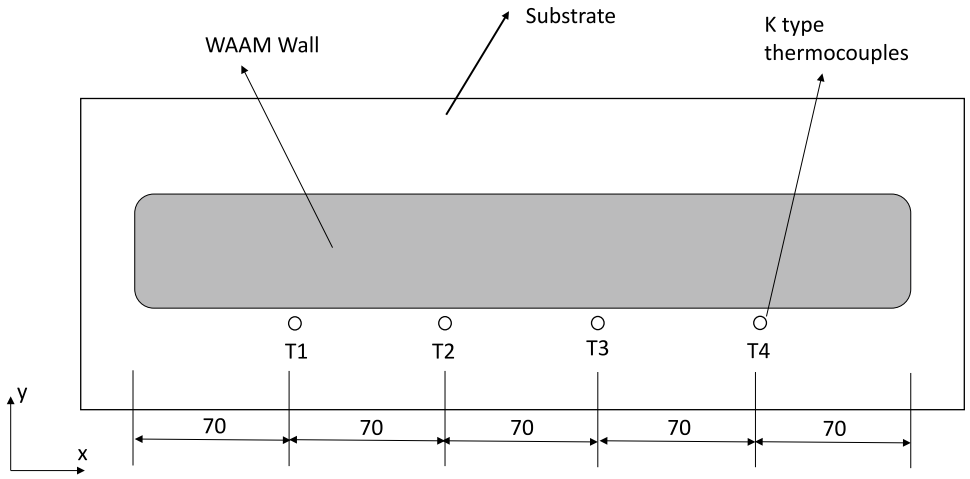


**Fig. 3** A schema of the top view of the position of the thermocouples in the substrate (dimensions in mm). T1 thermocouple 1, T2 thermocouple 2, T3 thermocouple 3, T4 thermocouple 4

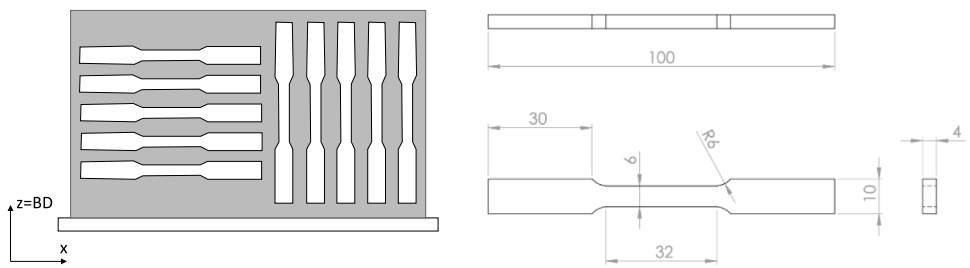


**Fig. 4** Scheme of the specimens (front view) for tensile test extracted from different walls

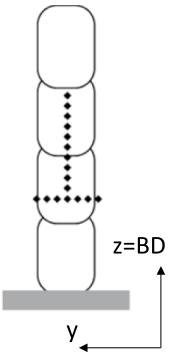


**Fig. 5** Scheme of the position of the hardness measurements (side view) done in the walls with different strategies

measurements done was dependent on the layer height and the wall thickness, as can be seen in Fig. 5.

To perform dilatometry tests, three specimens per manufacturing strategy were machined in the growth direction of the walls. Specimens were cylinders of 3 mm diameter and 10 mm length, as shown in Fig. 6. Dilatometry tests were done according to ASTM E831-14 standard using a Linseis L75 Platinun series high-temperature dilatometer, Linseis Messgeräte GmbH, Selb, Germany. The samples were heated to 1000 °C at a heating rate of 5 °C/s. Then, the samples were cooled down to room temperature. The linear voltage displacement transducer (LVDT) measures the linear deflection (DL) using push rods attached to the final part of the sample. To measure the temperature during the process, a thermocouple is welded to the sample.

## 3 Results

Using the mentioned strategies, the following walls were obtained: single weld bead (Fig. 7a), circular single weld bead (Fig. 7b), meandering weld bead (Fig. 7c), and three overlapped weld beads (Fig. 7d). The front view and top view can be seen in each one, where resulting thicknesses are shown: 4 mm for the single weld bead strategy, 5.8 mm for the circular single weld bead strategy, 21.5 mm for the meandering strategy, and 10.5 mm for the three overlapped weld beads strategy.

### 3.1 Thermal characterization

In Fig. 8, results recorded by the four thermocouples (T1, T2, T3, and T4) for the single weld bead manufacturing

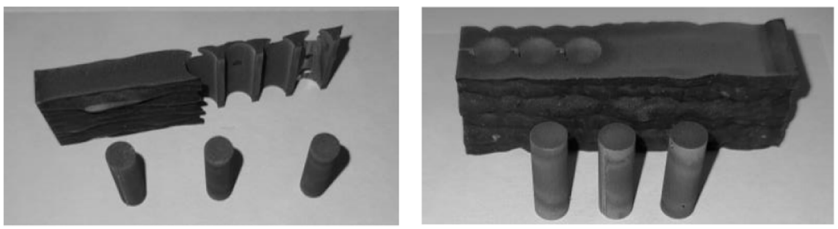

**Fig. 6** Example of dilatometry specimens obtained from WAAM walls with different manufacturing strategies

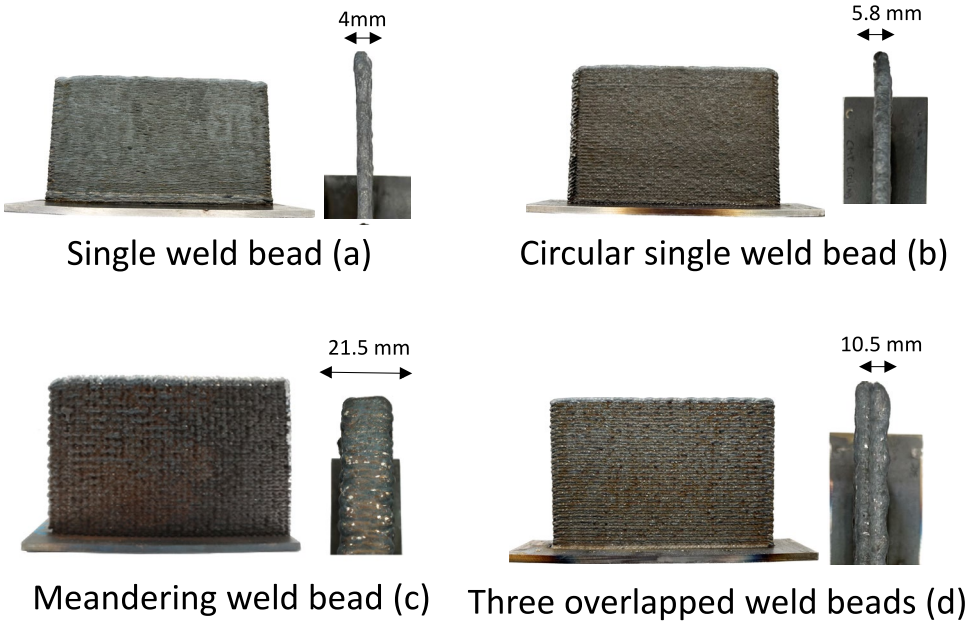


**Fig. 7** Front view and top view of the manufactured WAAM walls: **a** single weld bead, (**b**) circular single weld bead, (**c**) meandering weld bead, and (**d**) three overlapped weld beads

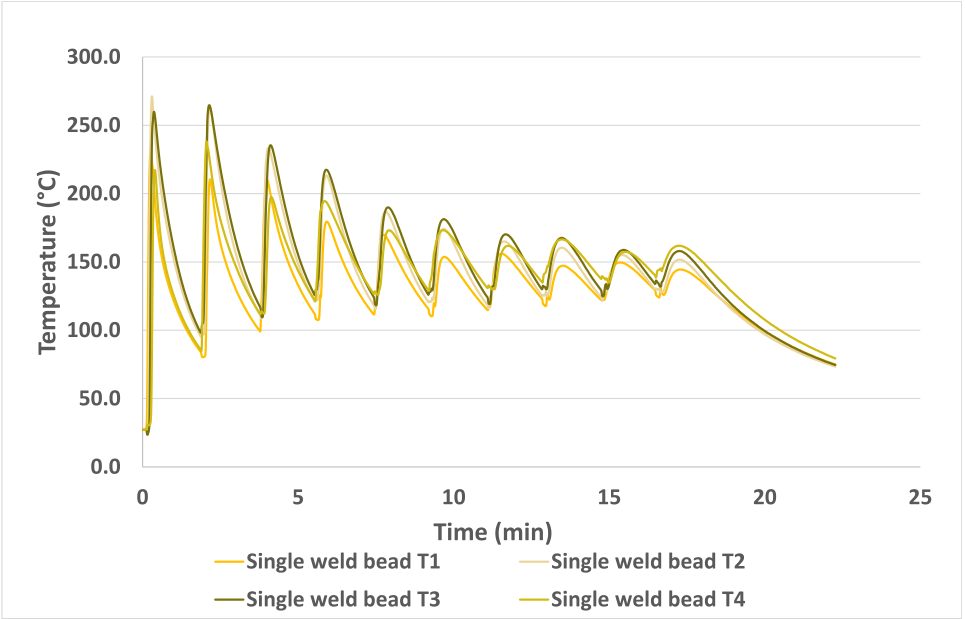


**Fig. 8** Temperature records for Single weld bead by T1, thermocouple 1; T2, thermocouple 2; T3, thermocouple 3; and T4, thermocouple 4

strategy can be seen. The same effect of temperature difference recorded between the four thermocouples is observed for the four deposition strategies. In order to facilitate the comparison between the four strategies and to make the data presentation clearer, the comparison has been made taking into account in all cases the data recorded by thermocouple 1.

In Fig. 9, the temperature recording of each manufacturing strategy can be seen: single weld bead, circular single weld bead, meandering weld bead, and three overlapped weld beads. The results shown are recorded by the T1, thermocouple 1. The repeated heating and cooling cycles typical of this manufacturing process can be seen. The registered temperature shows very clearly the differences on the thermal input for each manufacturing strategy, having the highest temperatures in the meandering weld bead strategy and the lowest temperature in the single weld bead strategy.

## 3.2 Morphological characterization

In Table 5 and Fig. 10, the effective area in percentage and the BTF ratio of the different strategies are shown. Figure 11 shows the total area and the effective area obtained from a cross section of a wall. The total area (Fig. 11, red line) is the one obtained directly by the manufacturing, and the effective area (Fig. 11, green line) is the largest rectangular that can be shaped in the cross section, the area that can be achieved machining the external waves that are typically obtained in this manufacturing method.

## 3.3 Microstructural characterization

A detailed cross section of the different strategy, single-, circular single-, meandering, and three overlapped weld beads, walls is shown in Fig. 12. In all cases, the fusion lines of the subsequently deposited layers are appreciated. In all cases, elongated large grains that grow in the growing direction can be seen. In the case of meandering and three overlapped weld beads, the orientation of the grains is more complicated, due to a more complicated heat history. In general, the columnar grains extend through multiple layers.

Complementary microstructural analysis was carried out by light optical microscopy (LOM). The substructure comprises cellular and columnar dendrites. Similar substructures were observed in different strategies, substructures that can be observed along the entire length of the walls. The observed substructures can be seen in Fig. 13.

Figure 14 a, b, c, and d shows EBSD inverse pole figure (IPF) maps of the different strategies analyzed: (a) single weld bead strategy wall, (b) circular single weld bead strategy wall, (c) meandering weld bead strategy wall, (d) three overlapped weld beads strategy wall. Fundamental differences in the microstructures can be seen regarding grain morphology and crystal orientation. The circular single weld bead strategy (b) and meandering weld bead strategy (c) are characterized by a columnar-grained structure aligned parallel to the build direction, with widths of 90–650 µm for strategy (b) and 200–950 µm and length of several millimeters for strategy (c). In the meandering weld bead case (c), a preferred crystallographic orientation (001) respecting the build direction can be seen, due to the high quantity

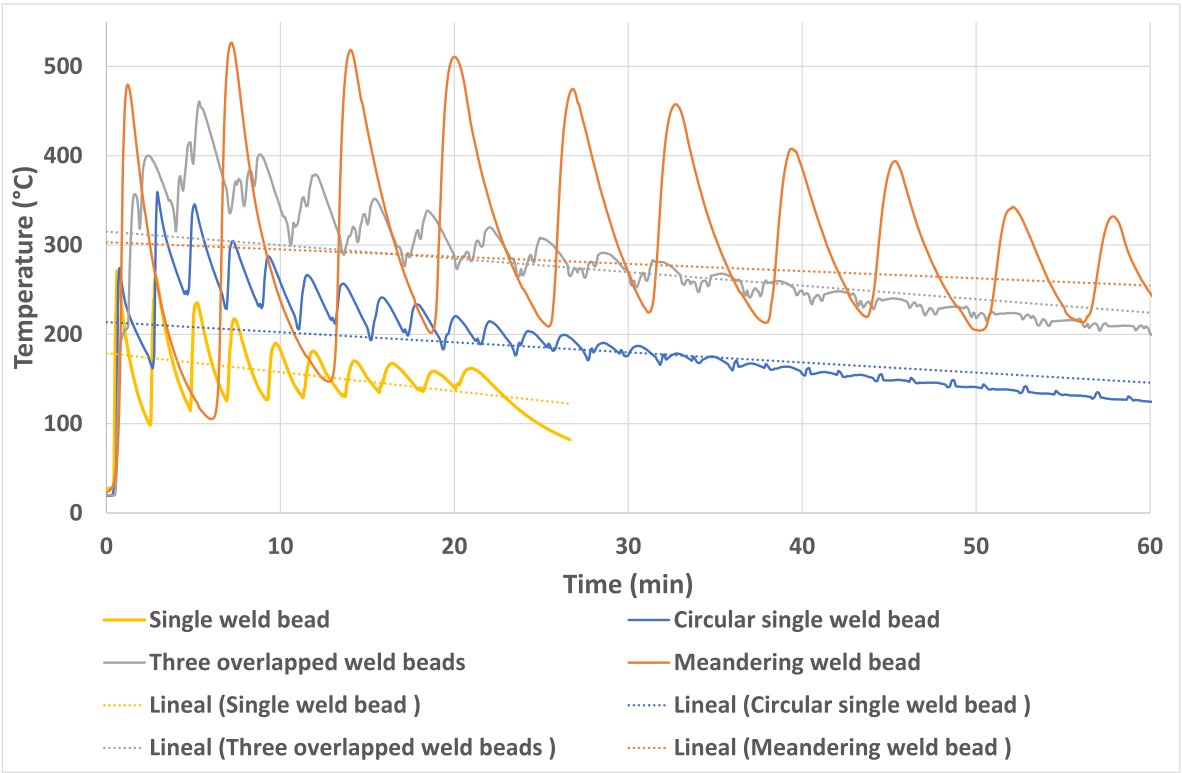


**Fig. 9** Temperature records by T1, thermocouple 1, for single weld bead, circular single weld bead, three overlapped weld beads, and meandering weld bead

**Table 5** Calculated effective area and BTF for different strategies

| Strategies used | Effective area (%) Without waving | BTF ratio Total area/ effective area |
|---|---|---|
| Single weld bead | 81.0 | 1.23 |
| Circular single weld bead | 81.2 | 1.23 |
| Meandering weld bead | 92.5 | 1.08 |
| Three overlapped weld beads | 87.6 | 1.14 |

of grains in shades of red. In the circular single weld bead strategy (b), the crystallographic orientation goes from (001) to (101). In single weld bead (a), the grained structure is also aligned parallel to the build direction, but the width of the grains is lower in this case (135–410 µm), and there is no preferred crystallographic orientation. Last, but not least, in the three overlapped welds bead (d), the columnar grains are not orientated in the build direction. The grain size differs depending on the zone of the wall, being smaller in the wall edges (920–70 µm). In the middle zone of the wall, a greater ordering of the crystallographic orientation is perceived, since a zone where the misalignment between grains is less than 5° is detected. The crystallographic orientation does not have a specific texture according to the results obtained.

In addition to the EBSD analysis, EDS elemental measurements were performed. Similar results were obtained in the four strategy cases. Figure 15 shows the result for the single weld bead wall, where it can be observed that the chemical composition of the precipitated phase substantially differs from the Fe–Ni matrix, being this precipitated phase enriched in Nb.

### 3.4 Mechanical characterization

Table 6 shows the summary of mechanical properties obtained for the samples single-, circular single-, meandering, and three overlapped weld beads. Average values for all samples and standard deviations are given. Mechanical properties were obtained for the *Z* (vertical direction) and *X* (horizontal direction) directions. Anisotropy was also appreciable with consistently higher strength and lower elongation in the horizontal direction, except in the meandering weld bead wall, where the higher strength and lower elongation are obtained in the vertical direction. The results revealed that the higher strength is obtained in three overlapped weld bead walls, having in this case the lowest elongation.

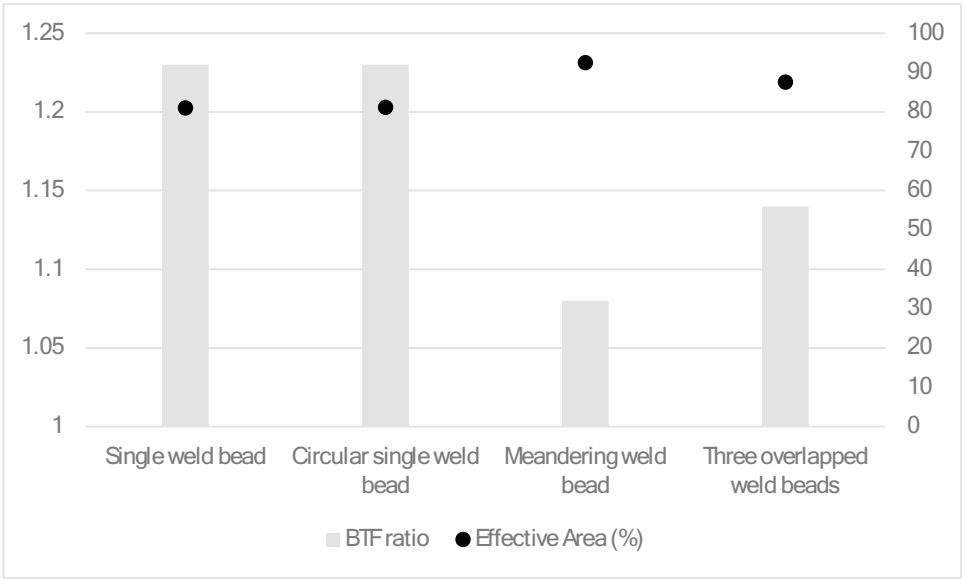


**Fig. 10** Graphical representation of the BTF ratio and the effective areas of the four different strategies

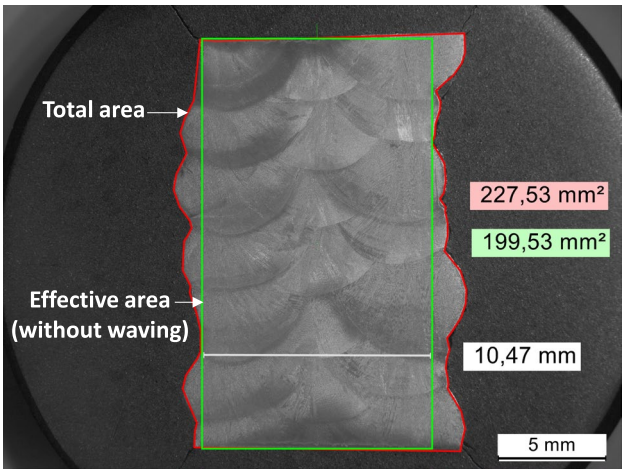


**Fig. 11** Example of cross section of a three overlapped weld bead WAAM wall where total area and effective area without waving are indicated

### 3.5 Hardness

Hardness measurement tests were carried out in the cross sections on the *Z* (vertical or build direction) and *X* (horizontal or transverse direction) directions to find differences between the analyzed strategies (Table 7). As can be seen, the deposition strategy has an evident effect in the hardness and ductility of the samples, having the hardest hardness of the wall deposited using the single weld bead strategy and the lowest the three overlapped weld bead strategy. There is no hardness difference between the orientations (Fig. 16).

### 3.6 Dilatometry analysis

Dilatometry tests were performed in the *Z* direction (vertical direction) to determine differences between the analyzed strategies. Three specimens were taken in the analyzed direction from each wall manufactured utilizing the

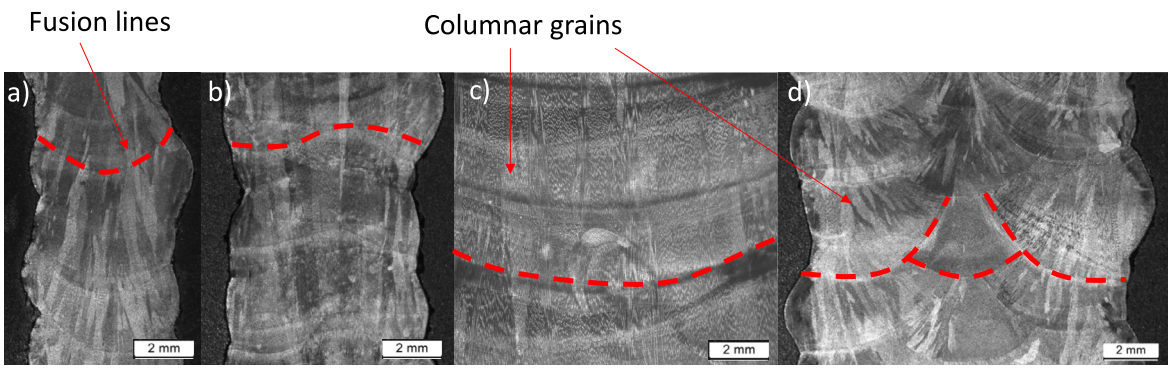


**Fig. 12** Cross section of WAAM walls after destructive testing: **a** single weld bead strategy wall, (**b**) circular single weld bead strategy wall, (**c**) meandering weld bead strategy wall, and **d** three overlapped weld beads strategy wall

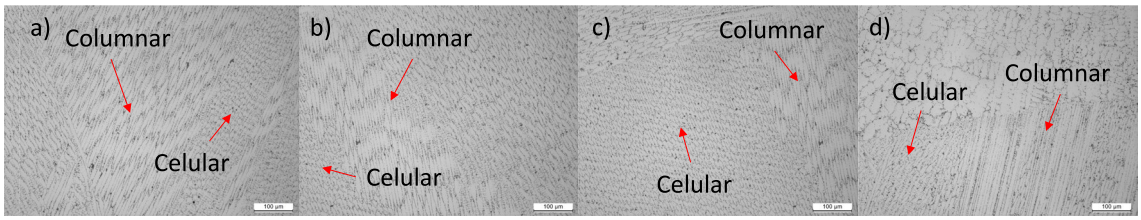


**Fig. 13** LOM micrographs for substructure analysis of WAAM walls: **a** single weld bead strategy wall, (**b**) circular single weld bead strategy wall, (**c**) meandering weld bead strategy wall, and (**d**) three overlapped weld beads strategy wall

four manufacturing strategies. In the dilatometry test, the material is heated and cooled in a controlled mode. Then, the linear deflection of the specimens is measured. The following (Eq. 2) is used to calculate the CTE ($10^{-6}$ °$C^{-1}$):

$$CTE = \alpha = \frac{\Delta L}{L_0 \times \Delta T} \tag{2}$$

where $\Delta L$ is the linear deflection, $L_0$ is the initial length of the specimen, and $\Delta T$ is the temperature difference.

The medium heating curves obtained from the dilatometry tests of samples machined from the walls produced using the four different strategies are shown in Fig. 17. As can be seen, similar curves were obtained, except in the meandering case, where the thermal expansion is higher. Aldalur et al. [25] compare the dilatometry of the GMAW-based and PAW-based WAAM Invar results with laminated Invar material. In this study, expansion values of around 50 microns are obtained at 400 °C, while Aldalur et al. [25] achieve an expansion of around 40 µm for both manufacturing processes.

The evolution of the CTE value with respect to temperature is shown in Fig. 18. Similar CTE values were obtained in the specimens manufactured with different strategies, except in the case of meandering, in which the CTE values increase more with temperature; this may be due to a higher thermal input in manufacturing. Even so, comparing these results with the ones obtained by Aldalur et al. [25], CTE values are lower for the strategies analyzed in this work.

## 4 Discussion

In this study, the influence of the manufacturing strategy (torch movement) for different Invar36 WAAM wall thicknesses has been investigated.

The thermal characterization showed that the heat depends on the strategy used and, therefore, the amount of deposited material. Although the difference in instantaneous heat input is not remarkable between the strategies, the way in which the material is deposited in each strategy causes the accumulated heat to vary. The relation between the heat accumulation and the wall thickness achieved is clear, having more heat accumulated in the thicker wall manufactured by meandering weld bead strategy. The differences in the thermal cycles suggested that there will be differences in the obtained microstructures and, therefore, in the properties obtained.

If the relationship between the strategy and the manufacturing temperature recorded with the microstructure obtained is considered, it can be observed that the higher the manufacturing temperature, which in this study is given in the meandering weld bead strategy, the more ordered microstructure is obtained. The high temperatures allow the grains to orient themselves in the direction of wall growth. In the case of three overlapped welds bead strategy, even though the temperature recorded is high, the orientation applied when depositing the strands means that the grains do not grow in an orientation parallel to the wall growth. It should be noted that none of the four strategies used had defects such as cracks or lack of fusion observed.

The mechanical properties of the strategies analyzed in this work are comparable with the literature studies on WAAM manufacturing of the Invar 36 [12, 26, 27], with LMD powder manufacturing [24], and comparing with commercial Invar (UTS = 448 MPa, $e$ = 35% [28]), the different strategies has better yield strength and ultimate tensile strength but less elongation, which is a typical correlation between strength and ductility in Fe-based alloys.

Although the mechanical properties are comparable with the ones reported in the bibliography [12, 26, 27], small differences in mechanical properties between strategies are detected which are related to the microstructure of each strategy. The EBSD analysis shows differences in the orientation of the columnar grains, and preferred crystallographic orientation differs between strategies. The best results in terms of mechanical properties are obtained in three overlapped welds bead strategy, having this a microstructure of columnar grains not orientated in the build direction and not a specific crystallographic texture. By contrast, the worst mechanical properties are obtained in the strategy that has a columnar grained structure aligned parallel to the build direction and has a preferred crystallographic orientation, being this the meandering weld bead strategy. The difference

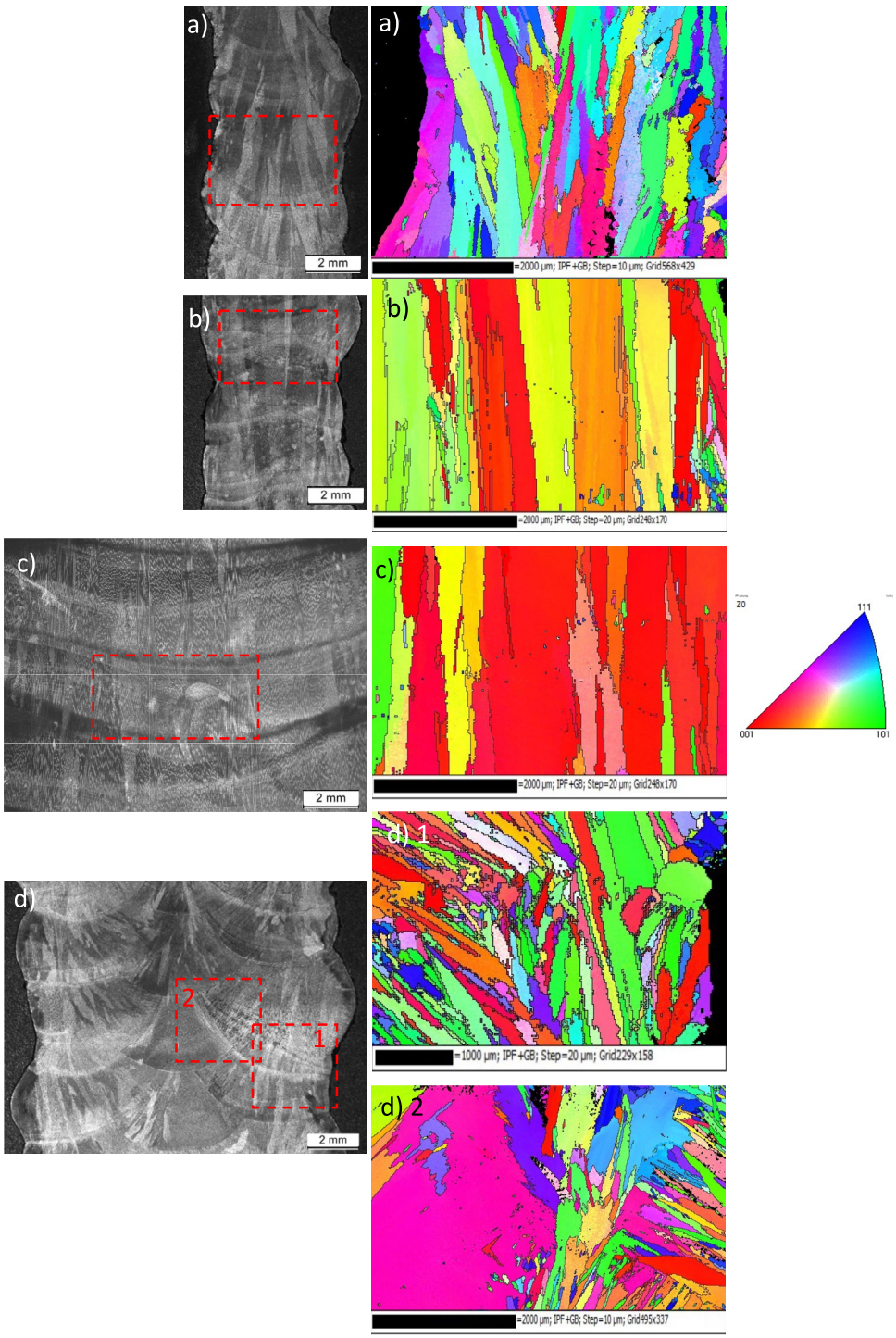


**Fig. 14** EBSD inverse pole figure (IPF) maps of (**a**) single weld bead strategy wall, (**b**) circular single weld bead strategy wall, (**c**) meandering weld bead strategy wall, and (**d**) three overlapped weld beads strategy wall. The grain orientations (see standard triangle) are plotted with respect to the built direction (vertical)

between the mechanical properties of the different strategies depends on the behaviour of the grains at the moment a stress is applied; it depends on the movement generated between adjacent grains. Liu et al. [29] concluded that the mechanical anisotropy was strongly associated with grain movements through different dominant deformation mechanisms in different building directions in stainless steel parts obtained by selectively laser melted (SLM). As in the aforementioned work, the present work concludes that the grains have undergone a highly dynamic movement during the tensile tests. In the case of three overlapped welds bead strategy, as the grains are not orientated, the grains have undergone a rotation, which increases the tensile strength, but without elongation of the grains, obtaining lower elongation values. In contrast, the meandering weld bead strategy involves grain elongation via dislocation slipping in the

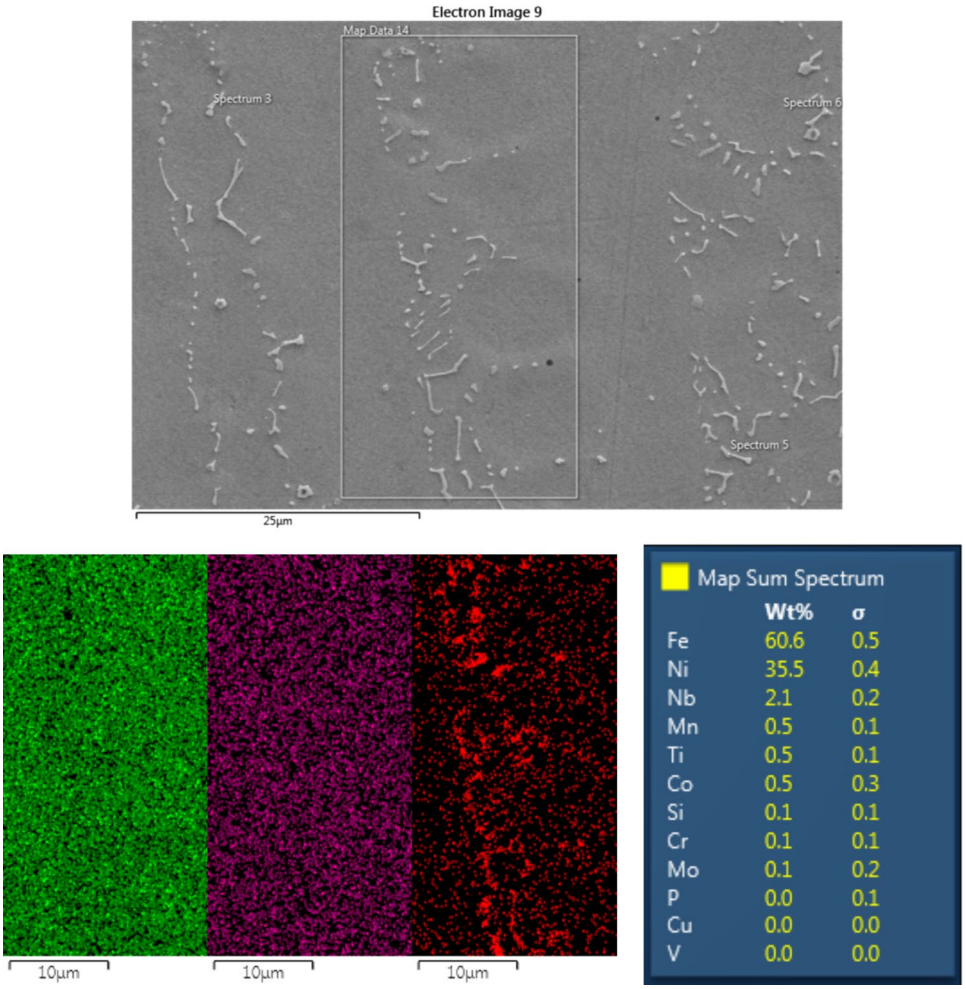


**Fig. 15** Single weld bead wall FESEM Micrograph (SE mode, 2000×) in the top, EDS elemental measurement where Fe–Ni matrix and precipitated phase enriched in Nb is shown (down left) and percentage measurement of each element (down right)

**Table 6** Mechanical properties (*Rp0.2* yield strength, *Rm* ultimate tensile strength, *e* elongation) achieved for both orientations for WAAM parts manufactured using different strategies

| Strategies used | Orientation | Rp0.2 (MPa) | Rm (MPa) | *e* (%) |
|---|---|---|---|---|
| Single weld bead | *Z* | 318 ± 6.5 | 481 ± 6.9 | 27 ± 1.2 |
| | *X* | 329 ± 4.3 | 489 ± 5.7 | 23 ± 1.4 |
| Circular single weld bead | *Z* | 310 ± 3.6 | 460 ± 1.6 | 30 ± 1.6 |
| | *X* | 339 ± 4.2 | 484 ± 1.4 | 27 ± 1.9 |
| Meandering weld bead | *Z* | 319 ± 3.1 | 467 ± 0.6 | 26 ± 0.3 |
| | *X* | 285 ± 3.6 | 439 ± 3.5 | 30 ± 2.6 |
| Three overlapped weld beads | *Z* | 326 ± 5.6 | 514 ± 4.5 | 23 ± 3.8 |
| | *X* | 382 ± 1.4 | 581 ± 0.8 | 20 ± 1.5 |
| Bibliography reference [12, 26] | *Z* | 305 | 464 | 33 |
| | *X* | 345 | 505 | 29 |

**Table 7** Microhardness values for the different strategies in the *Z* (vertical direction) and *X* (horizontal direction) directions

| Strategies used | Orientation | HV0.1 |
|---|---|---|
| Single weld bead | *Z* | 206 ± 12.0 |
| | *X* | 205 ± 8.6 |
| Circular single weld bead | *Z* | 184 ± 8.3 |
| | *X* | 191 ± 10.0 |
| Meandering weld bead | *Z* | 181 ± 8.7 |
| | *X* | 180 ± 4.4 |
| Three overlapped weld beads | *Z* | 174 ± 5.3 |
| | *X* | 175 ± 6.0 |

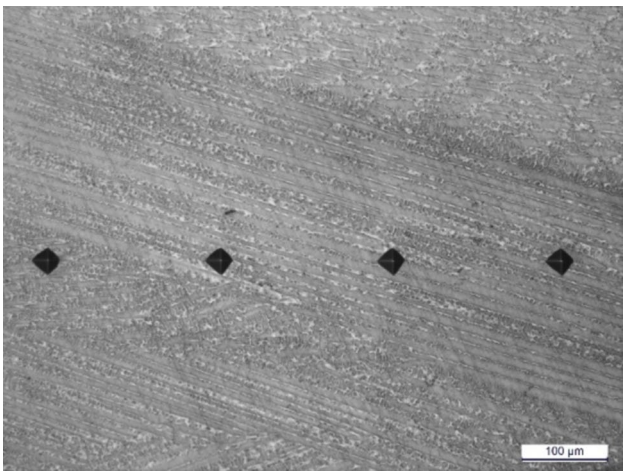


**Fig. 16** Example of the indentations done in one of the samples

*Z*-direction tensile tests and grain elongation and rotation in the *Y*-direction. The same reasoning is applicable to the anisotropy detected between the two directions (*Y*, *Z*) in each strategy. In terms of substructure, cellular and columnar dendrites are observed in different strategies with no significant differences.

At the microstructural level when comparing the width of columnar grains obtained via WAAM (arc deposition) with those produced by another DED process using laser and powder for a similar Invar alloy [24], it is observed that both processes, under a similar deposition strategy (i.e., single weld bead deposition, strategy a), produce columnar grain structures aligned parallel to the build direction (Z-axis). However, with WAAM, a maximum grain width of 410 µm was obtained, while the LMD process reports grain widths around 300 µm [24]. This suggests that the columnar grain size obtained with WAAM is larger.

In terms of hardness, the obtained results are comparable with those observed in other studies [27, 30]. As in the case of mechanical properties, in the hardness results, small differences have been detected. In this case, the differences are related to the grain size and the manufacturing temperature, having the highest hardness result in the single weld bead strategy, being this the coolest process and the one that has the lowest grain width. On the other hand, the lowest hardness results are observed in the three overlapped weld bead, in which the manufacturing temperature, together with the meandering weld bead, is the highest, and grains with widths up to 2000 µm have been observed.

When comparing the hardness obtained in this research with values reported in the literature for similar material produced via the LMD powder process, it is observed that, in the *Z* direction and under the single weld bead strategy, higher hardness is achieved with the WAAM process compared to the LMD powder DED process [24], with values of 205 HV versus 150 HV, respectively. This difference is likely due to the distinct solidification conditions of the deposited materials, the temperature gradient, and slight variations in the chemical composition ranges.

Regarding the CTE values measured for the different deposition strategies, it is observed that the largest difference is found in the case of meandering weld bead, which is the case where the highest fabrication temperature was observed. Considering the results obtained by Aldalur et al. [25], in which the CTE results of the PAW process are higher than with GMAW and are related to a higher heat input in the PAW process, the same effect is being observed in the case of meandering weld bead. In the same way that Kahlert et al.[31] do not see an influence of the microstructure on the CTE values, in this work, this influence is not detected, since having a different microstructure between deposition strategies, similar CTE values are obtained, always with the exception of the meandering weld bead strategy.

## 5 Conclusions

In this study, Invar 36 WAAM manufactured parts were obtained using four different deposition strategies, having small differences in the analyzed properties:

- The heat accumulation depends in the instantaneous heat input and the way and quantity that the material is deposited in each manufacturing strategy.
- The heat accumulation makes the microstructure obtained more ordered, unless the material deposition is made at an angle that makes the grains grow in a direction other than the direction of columnar growth.
- The four different strategies used to manufacture the walls have resulted in slight differences in the microstructure and mechanical properties obtained. Both the granular alignment and the crystallographic texture obtained from each strategy affect the mechanical properties, due

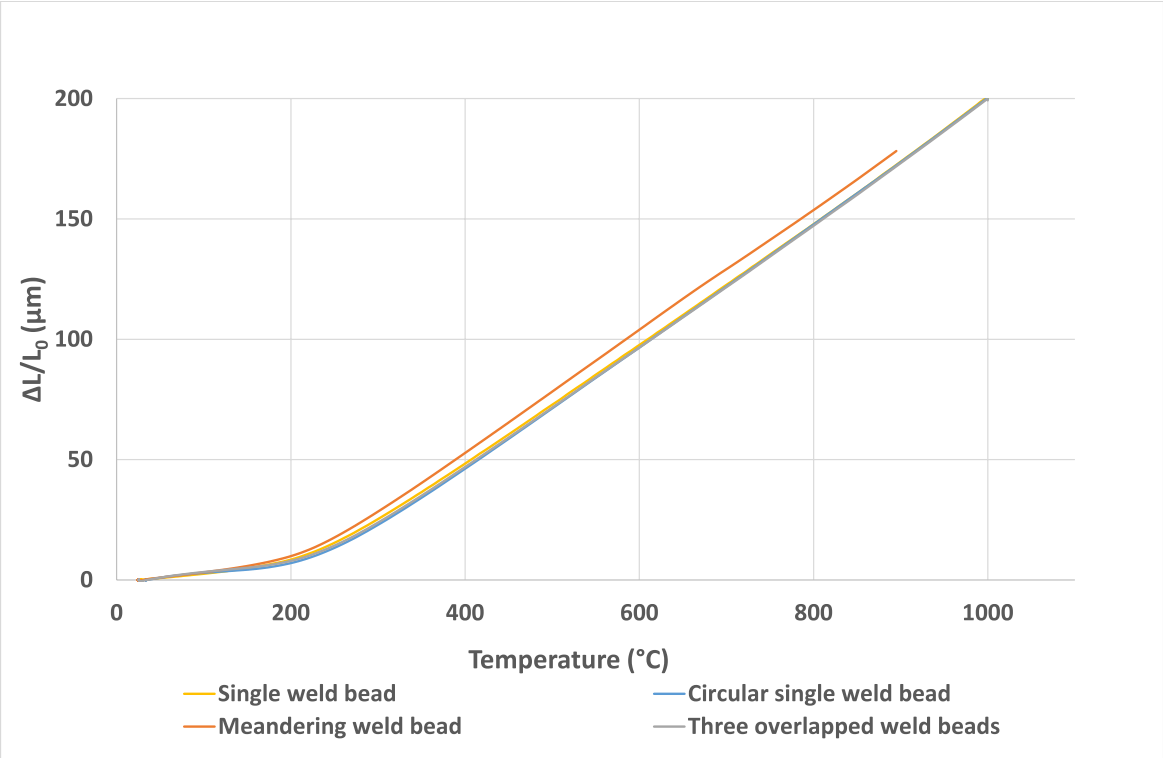


**Fig. 17** Dilatometry curves of the specimens taken from the wall manufactured using the strategies **a** single weld bead, **b** circular single weld bead, **c** meandering weld bead, and **d** three overlapped weld beads

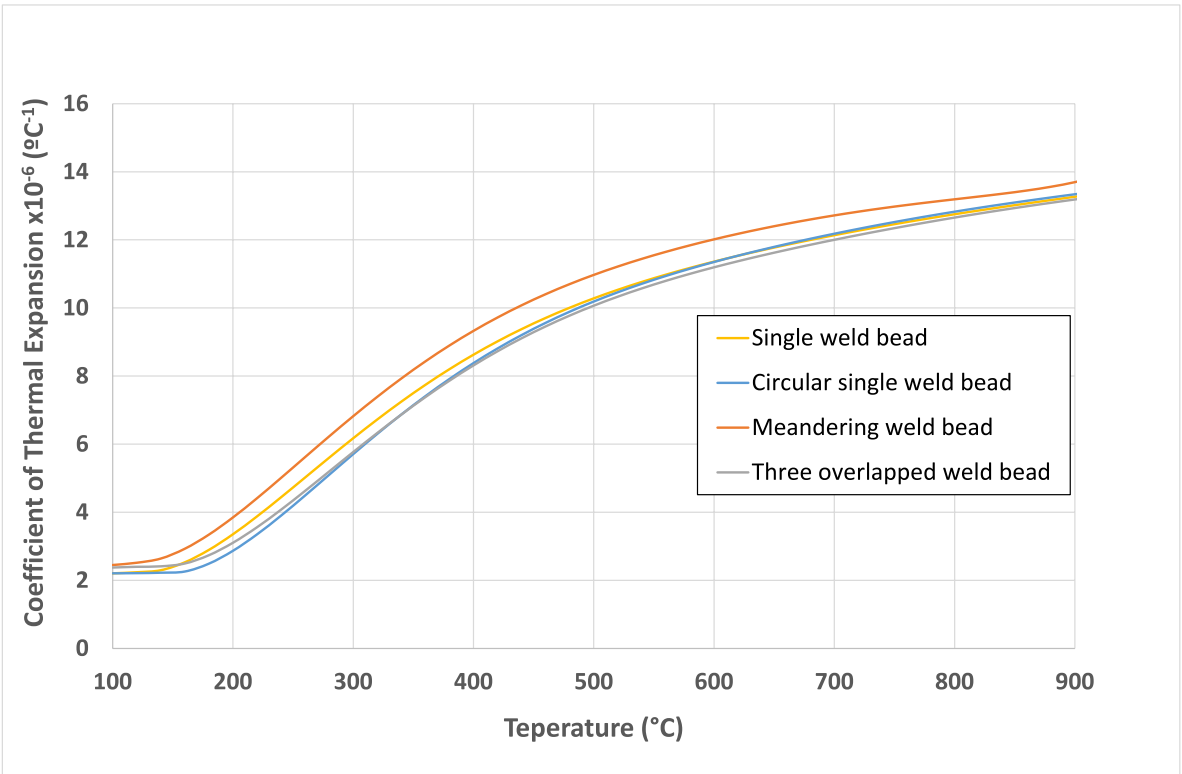


**Fig. 18** CTE value evolution in relation to temperature

to inter-grain displacement mechanisms that affect differently in each case.

- The result of the hardnesses depends on the thermal gradient of the manufacturing process, which is different for each manufacturing strategy, and the grain size resulting from these different thermal gradients.
- The coefficient of thermal expansion is not affected by the microstructure obtained by the different deposition strategies but by the thermal input of the strategy, obtaining worse results in the strategy with higher heat accumulation, as is the case with the meandering weld bead strategy.

**Funding** Open Access funding provided thanks to the CRUE-CSIC agreement with Springer Nature. This research work was supported by the Basque Government (Departamento de Desarrollo Económico e Infraestructuras, Programa ELKARTEK) through the REIMAGIN project (grant KK-2023/00096). And financed by the CDTI and the European Union—NextGenerationEU and supported by the Ministerio de Ciencia e Innovación within the project "MADISON—MANUFACTURA ADITIVA, DIGITALIAZACIÓN Y SOSTENIBILIDAD", approved within the framework of the call "Programa Cervera para Centros Tecnológicos 2023″ with Grant Agreement EXP—00163686 / CER-20231012".

**Data availability** The raw/processed data required to reproduce these findings cannot be shared at this time due to technical or time limitations.

**Code availability** Not applicable.

## Declarations

**Ethics approval** Not applicable.

**Consent to participate** All authors give their permission to participate and disseminate this work.

**Consent for publication** All authors give their authorization to publish this work.

**Conflict of interest** The authors declare no competing interests.



## References

1. ISO/TC 261 Additive manufacturing Technical Committee (2021) ISO/ASTM 52900:2021 Additive manufacturing — general principles — terminology. https://www.iso.org/standard/74514.html
2. Svetlizky D, Das M, Zheng B et al (2021) Directed energy deposition (DED) additive manufacturing: physical characteristics, defects, challenges and applications. Mater Today 49:271–295. https://doi.org/10.1016/j.mattod.2021.03.020
3. Mohd Mansor MS, Raja S, Yusof F et al (2024) Integrated approach to wire arc additive manufacturing (WAAM) optimization: harnessing the synergy of process parameters and deposition strategies. J Mater Res Technol 30:2478–2499. https://doi.org/10.1016/j.jmrt.2024.03.170
4. Kumar A, Maji K (2020) Selection of process parameters for near-net shape deposition in wire arc additive manufacturing by genetic algorithm. J Mater Eng Perform 29:3334–3352. https://doi.org/10.1007/s11665-020-04847-1
5. Baier D, Wolf F, Weckenmann T et al (2022) Thermal process monitoring and control for a near-net-shape wire and arc additive manufacturing. Prod Eng 16:811–822. https://doi.org/10.1007/s11740-022-01138-7
6. Rodriguez N, Vázquez L, Huarte I et al (2018) Wire and arc additive manufacturing: a comparison between CMT and TopTIG processes applied to stainless steel. Weld World 62:1083–1096. https://doi.org/10.1007/s40194-018-0606-6
7. Fronius Company (2024) CMT - procesos de soldadura - tecnología de soldadura - Fronius. https://www.fronius.com/es-es/spain/tecnologia-de-soldadura/el-mundo-de-la-soldadura/fronius-welding-processes/cmt
8. Vazquez L, Rodriguez MN, Rodriguez I, Alvarez P (2021) Influence of post-deposition heat treatments on the microstructure and tensile properties of ti-6al-4v parts manufactured by cmt-waam. Metals (Basel) 11:1161. https://doi.org/10.3390/met11081161
9. Suat Y, Koc B, Yilmaz O (2020) Building strategy effect on mechanical properties of high strength low alloy steel in wire + arc additive manufacturing. Zavar i zavarene Konstr 65:125–136. https://doi.org/10.5937/zzk2003125s
10. Yan L (2013) Wire and arc additive manufacture (WAAM) reusable tooling investigation. Crandfield University
11. Arbogast A, Roy S, Nycz A et al (2020) Investigating the linear thermal expansion of additively manufactured multi-material joining between Invar and steel. Materials (Basel) 13:5683
12. Veiga F, Suárez A, Artaza T, Aldalur E (2022) Effect of the heat input on wire-arc additive manufacturing of Invar 36 alloy: microstructure and mechanical properties. Weld World 66:1081–1091. https://doi.org/10.1007/s40194-022-01295-4
13. Sood A, Schimmel J, Ferreira VM et al (2023) Directed energy deposition of Invar 36 alloy using cold wire pulsed gas tungsten arc welding: effect of heat input on the microstructure and functional behaviour. J Mater Res Technol 25:6183–6197. https://doi.org/10.1016/j.jmrt.2023.06.280
14. Silva MIC e (2018) Study of deposition strategies of a wire + arc additive manufactured component materials engineering. Técnico Lisboa
15. Vo HT, Grandvallet C, Vignat F (2021) A model for manufacturing large parts with WAAM technology. Adv Transdiscipl Eng 15:79–84. https://doi.org/10.3233/ATDE210016
16. Müller J, Hensel J (2023) WAAM of structural components—building strategies for varying wall thicknesses. Weld World 67:833–844. https://doi.org/10.1007/s40194-023-01481-y
17. Ding D, Pan Z, Cuiuri D, Li H (2015) A practical path planning methodology for wire and arc additive manufacturing of

thin-walled structures. Robot Comput Integr Manuf 34:8–19. https://doi.org/10.1016/j.rcim.2015.01.003
18. Ding D, Pan Z, Cuiuri D, Li H (2015) Process planning strategy for wire and arc additive manufacturing. In: Advances in intelligent systems and computing, pp v–vi. https://doi.org/10.1007/978-3-319-18997-0_37
19. Lezaack M, Nunes R, Verlinde W, Simar A (2023) Understanding the influence of WAAM deposition strategy on mechanical properties and damage mechanisms of 5183 and 2219 Al alloys. In: "THERMEC 2023", Vienne, Autriche
20. Frimpong Ayarkwa K, Pinter Z, Eimer E et al (2021) Effect of the deposition strategy on Al - Cu alloy wire + arc additive manufacture. Mater Sci Technol (United Kingdom) 1:28–34
21. Arana M, Ukar E, Rodriguez I et al (2022) Influence of deposition strategy and heat treatment on mechanical properties and microstructure of 2319 aluminium WAAM components. Mater Des 221:110974. https://doi.org/10.1016/j.matdes.2022.110974
22. Rauch M, Nwankpa UV, Hascoet JY (2021) Investigation of deposition strategy on wire and arc additive manufacturing of aluminium components. J Adv Join Process 4:100074. https://doi.org/10.1016/j.jajp.2021.100074
23. Cong B, Qi Z, Qi B et al (2017) A comparative study of additively manufactured thin wall and block structure with Al-6.3%Cu alloy using cold metal transfer process. Appl Sci 7:275. https://doi.org/10.3390/APP7030275
24. Li H, Chen B, Tan C et al (2020) Microstructure evolution and mechanical properties of laser metal deposition of Invar 36 alloy. Opt Laser Technol 125:106037. https://doi.org/10.1016/j.optlastec.2019.106037
25. Aldalur E, Suárez A, Veiga F (2022) Thermal expansion behaviour of Invar 36 alloy parts fabricated by wire-arc additive manufacturing. J Mater Res Technol 19:3634–3645. https://doi.org/10.1016/j.jmrt.2022.06.114
26. Gil Del Val A, Cearsolo X, Suarez A et al (2023) Machinability characterization in end milling of Invar 36 fabricated by wire arc additive manufacturing. J Mater Res Technol 23:300–315. https://doi.org/10.1016/j.jmrt.2022.12.182
27. Jiao G, Fang X, Chen X et al (2023) The origin of low thermal expansion coefficient and enhanced tensile properties of Invar alloy fabricated by directed energy deposition. J Mater Process Technol 317:117994. https://doi.org/10.1016/j.jmatprotec.2023.117994
28. Zheng S, Sokoluk M, Yao G et al (2019) Fe–Ni Invar alloy reinforced by WC nanoparticles with high strength and low thermal expansion. SN Appl Sci 1:1–6. https://doi.org/10.1007/s42452-019-0182-4
29. Liu Q, Wang G, Qiu C (2020) On the role of dynamic grain movement in deformation and mechanical anisotropy development in a selectively laser melted stainless steel. Addit Manuf 35:101329. https://doi.org/10.1016/j.addma.2020.101329
30. Eissel A, Engelking L, Gustus R et al (2023) Alloy modification for additive manufactured Ni alloy components—part I: effect on microstructure and hardness of Invar alloy. Weld World 67:1049–1057. https://doi.org/10.1007/s40194-023-01510-w
31 Kahlert M, Wegener T, Laabs L et al (2024) Influence of defects and microstructure on the thermal expansion behavior and the mechanical properties of additively manufactured Fe-36Ni. Materials (Basel) 17:4313. https://doi.org/10.3390/ma17174313